JOURNAL OF OPTOELECTRONICS AND ADVANCED MATERIALS Vol. 27, Iss. 11 - 12, November - December 2025, p. 587 - 595

Exploring the structural and electronic properties of CeO_2 thin films: role of thickness, temperature, and oxygen vacancies

SELEN GUNAYDIN[1], ERHAN CENGIZ[2], IMRAN KANMAZ[3], GÖKHAN APAYDIN[3], HIDETOSHI MIYAZAKI[4], MESSAOUD HARFOUCHE[5], OSMAN MURAT OZKENDIR[6,*]

[1]Faculty of Eneginering and Natural Sciences, Bahceşehir University, Istanbul,34349, Turkiye
[2]Department of Fundamental Sciences, Rafet Kayış Engineering Faculty, Alanya Alaaddin Keykubat University, 07425, Alanya, Antalya, Turkiye
[3]Department of Physics, Science Faculty, Karadeniz Technical University, 61080, Trabzon, Turkiye
[4]Department of Physical Science and Engineering, Nagoya Institute of Technology, Nagoya 466-8555, Japan
[5]Synchrotron-light for Experimental Science and Applications in the Middle East (SESAME), Allan 19252, Jordan
[6]Department of Mathematical and Natural Sciences, Tarsus University, 33400 Tarsus, Turkiye

Systematic investigation of the temperature-dependent local arrangements in CeO_2 thin films and their direct impact on electronic properties is presented. Results revealed that thicker films promote oxygen vacancy formation, reducing Ce^{4+} to Ce^{3+} and modifying the local coordination. Furthermore, temperature-dependent EXAFS analysis uncovers a local structural rearrangement transition above 400 K, driven by thermal activation of oxygen vacancies. This rearrangement, occurring within a globally stable cubic framework, directly alters the hybridization between Ce 4f/5d and O 2p orbitals. Density Functional Theory (DFT) calculations corroborate the experimental findings, revealing an indirect bandgap of 1.60 eV as a result of orbital hybridization.

(Received April 18, 2025; accepted December 4, 2025)

Keywords: Cerium dioxide (CeO_2), Thin films, EXAFS, Electronic structure

1. Introduction

Cerium dioxide (CeO_2) thin films have emerged as a highly intriguing material due to their exceptional physicochemical properties and broad applicability across diverse technological domains. CeO_2 exhibits a wide bandgap (~3–3.6 eV), making it suitable for optoelectronic and UV-related applications, and a high dielectric constant (~23–52), which is advantageous for microelectronic devices. Its remarkable chemical stability, mechanical robustness, and excellent lattice compatibility with various substrates further enhance its utility. Additionally, CeO_2 demonstrates a favorable refractive index (~2.2–2.8) for optical applications, coupled with high transparency in the visible and near-infrared spectral regions [1–3]. Its strong adhesion to silicon (Si) substrates, combined with its resistance to mechanical wear and chemical degradation, makes it an ideal candidate for integration into complementary metal-oxide-semiconductor (CMOS) devices [3].

In recent years, CeO_2 thin films have been extensively employed in a wide range of applications, including catalysis [4], electrochemical systems [5], optical coatings [6], electronic devices [7], gas sensors [8], UV-blocking filters [9], and corrosion-resistant coatings [10, 11]. These applications leverage the unique combination of CeO_2's electronic, optical, and structural properties, underscoring its versatility as a functional material.

In this study, homogeneous and cost-effective CeO_2 thin films were fabricated using the spin coating method. Spin coating is a solution-based deposition technique that offers several advantages, including simplicity, low cost, and the ability to produce films with high uniformity and controlled thickness [12]. This method is particularly well-suited for large-scale production and allows for precise tuning of film properties by adjusting processing parameters such as spin speed, solution concentration, and annealing conditions.

The primary focus of this study is to explore the influence of film thickness on the electronic structure of CeO_2 thin films. To achieve this, X-ray absorption spectroscopy (XAS) was employed as a powerful analytical tool to probe the electronic properties of the films. XAS is highly sensitive to the local atomic and electronic environment, making it an invaluable technique for studying the electronic structure, chemical bonding, defect states, and local symmetry of dopant ions in materials. Its applications span diverse fields, including electrochemistry, catalysis, and materials science.

In this work, Ce L_3-edge XAS was utilized to investigate the electronic structure of CeO_2 thin films with varying thicknesses (7 nm, 20 nm, 55 nm, 62 nm, 87 nm, and 115 nm). The Ce L_3-edge is particularly sensitive to the oxidation state and local coordination environment of cerium ions, providing insights into the electronic interactions and defect chemistry of the material. Complementary X-ray diffraction (XRD) measurements were conducted to validate the structural characteristics of the films, ensuring a comprehensive understanding of the relationship between film thickness, electronic structure, and crystallinity.

While numerous studies have examined the properties of CeO_2 thin films, a systematic correlation between film thickness, thermal history, and the resulting local atomic and electronic structure remains less explored. Many investigations focus on a single parameter, such as doping or annealing temperature, often for a fixed film thickness. This study adopts a comprehensive, two-pronged approach: first, by fabricating a series of CeO_2 thin films with precisely controlled thicknesses (7 nm to 115 nm) to probe size-dependent effects; and second, by performing temperature-dependent EXAFS analysis (250 K to 500 K) to unravel the thermal stability and activation of local structural rearrangements. This dual-parameter strategy allows for a more generalized understanding of how CeO_2's functional properties are intrinsically linked to its dimensional and thermal processing history.

2. Experimental

CeO_2 precursor solutions were prepared to fabricate thin films of six distinct thicknesses. These solutions were uniformly coated onto crystalline silicon (c-Si) substrates using the spin coating method. The spin coating process was carried out at a rotational speed of 6000 rpm for 30 seconds to ensure homogeneous film deposition. Following the coating process, the thin films were dried in air at 200°C for 5 minutes to remove residual solvents and subsequently annealed at 400°C for 60 minutes to achieve crystallinity and enhance film stability.

The precursor solution for the CeO_2 thin films was prepared using cerium (III) chloride heptahydrate ($CeCl_3 \cdot 7H_2O$, 99% trace metals basis, Sigma-Aldrich) as the cerium source and ethyl alcohol as the solvent. To facilitate the chelation process and improve solution stability, 15 µl of 0.2 M citric acid monohydrate (Merck, 99.7%) was added to the solution. The mixture was homogenized using a magnetic stirrer for 30 minutes and aged for 24 hours to ensure complete dissolution and chemical uniformity. To enhance the adhesion and homogeneity of the coating on the c-Si surface, 75 µl of triethanolamine (97%) was added to 5 ml of the precursor solution. The solution was then stirred at 50°C for 30 minutes before being applied to the substrates.

Crystalline silicon (CZ-Si) p-type wafers with a thickness of 725 µm and dimensions of 1×1 cm^2 were used as substrates. To remove the naturally occurring silicon dioxide (SiO_2) layer on the wafer surfaces, the substrates were immersed in a 1:10 diluted hydrofluoric acid (HF) solution. After etching, the wafers were thoroughly rinsed with deionized water to eliminate residual acid. Further cleaning was performed in an ultrasonic bath using ethyl alcohol and deionized water for 15 minutes each to ensure a contaminant-free surface. Finally, the substrates were dried in air to prepare them for film deposition [13].

The crystalline and electronic structures of the CeO_2 thin films were characterized using X-ray diffraction (XRD) and X-ray absorption spectroscopy (XAS). XRD measurements were conducted at Karadeniz Technical University using a PANalytical X'Pert3 Powder diffractometer equipped with Cu Kα radiation ($\lambda = 1.54059$ Å). The XRD data were used to determine the crystal structure parameters, including lattice constants and phase purity, of the CeO_2 thin films.

XAS measurements were performed at the XAFS/XRF beamline of the SESAME synchrotron facility in Jordan. This beamline, located on the bending magnet of the SESAME storage ring, provides a high photon flux (10^9–10^{12} ph/s) and exceptional beam stability, making it ideal for high-resolution XAS studies. A double-crystal monochromator equipped with Si(111) crystals was used to access the XAS region with a fine energy step size of 0.001–0.0005 eV near the absorption edge (-10 eV to +30 eV). Room-temperature XAS measurements were conducted at the Ce L_3-edge (5692 eV) to probe the electronic structure of the CeO_2 thin films. Data were collected in fluorescence yield mode using a step-by-step scanning technique, with X-ray fluorescence detection performed using an energy-selective single-element silicon drift detector (SDD) from KETEK GmbH (Germany).

To complement the experimental findings, electronic structure calculations were performed using the Quantum Espresso (QE) package [14]. The calculations employed norm-conserving and ultrasoft pseudopotentials in the UPF format, with an energy cutoff of 503 eV. A k-point mesh of $4 \times 4 \times 4$ was used for sampling the Brillouin zone, ensuring accurate representation of the electronic properties of the cubic “Fm-3m” CeO_2 thin films.

Extended X-ray absorption fine structure (EXAFS) calculations were also conducted using the FEFF8.2 code to support the analysis of the Ce L_3-edge XAS data. Input files for the calculations were prepared using crystallographic data for the cubic “Fm-3m” unit cell of CeO_2, with lattice parameters $a = b = c = 5.327$ Å and atomic positions O (0.25, 0.25, 0.25) and Ce (0.0, 0.0, 0.0). The calculations focused on a 295-atom cluster (Ce, O) with a diameter of 10 Å, capturing the local atomic environment around the absorbing cerium atoms.

The EXAFS calculations were performed at elevated temperatures (250 K, 300 K, 350 K, 400 K, 423 K, 450 K, 473 K, and 500 K) to investigate the temperature-dependent electronic and structural properties of CeO_2. The primary objective was to identify potential thermal instabilities or temperature-dependent resistance in the material. By analyzing the EXAFS spectra, key parameters such as bond lengths, coordination numbers, and oxidation states were monitored as a function of temperature. This approach provided critical insights into the mechanisms underlying thermal degradation and electronic performance in CeO_2 thin films, offering a comprehensive understanding of their behavior under varying thermal conditions.

3. Results and discussion

Cerium, a rare earth metal belonging to the lanthanide series, has attracted considerable scientific interest due to its intriguing electronic and magnetic properties, which make it a promising candidate for applications in semiconductor oxides. The ground state electronic configuration of cerium, [Xe] $4f^1$ $5d^1$ $6s^2$, underscores the significance of its partially filled 4f and 5d orbitals in governing the material's electronic, optical, and catalytic properties. The presence of unoccupied 4f and 5d orbitals enables cerium to exhibit variable oxidation states, predominantly 3+ and 4+, which play a critical role in determining the chemical reactivity and electronic behavior of cerium-based compounds, such as cerium dioxide (CeO_2).

The crystal structures of the CeO_2 thin films were systematically investigated using X-ray diffraction (XRD) analysis, as illustrated in Fig. 1. The XRD patterns revealed highly symmetrical and well-defined diffraction peaks, indicative of the high crystallinity and structural stability of the films across varying thicknesses. The observed peaks correspond to the cubic fluorite structure (space group "Fm-3m"), which is characteristic of CeO_2. This structure consists of a face-centered cubic (fcc) arrangement of cerium ions, with oxygen ions occupying the tetrahedral interstitial sites.

Despite the overall structural stability, minor variations in peak intensities and slight shifts in peak positions were detected, which can be attributed to changes in the atomic composition and local strain within the films. These subtle alterations suggest that the composition and thickness of the films influence the lattice parameters and crystallographic orientation, albeit without disrupting the overall cubic symmetry. The lattice parameters derived from the XRD analysis are summarized in Table 1, providing quantitative insights into the structural properties of the CeO_2 thin films.

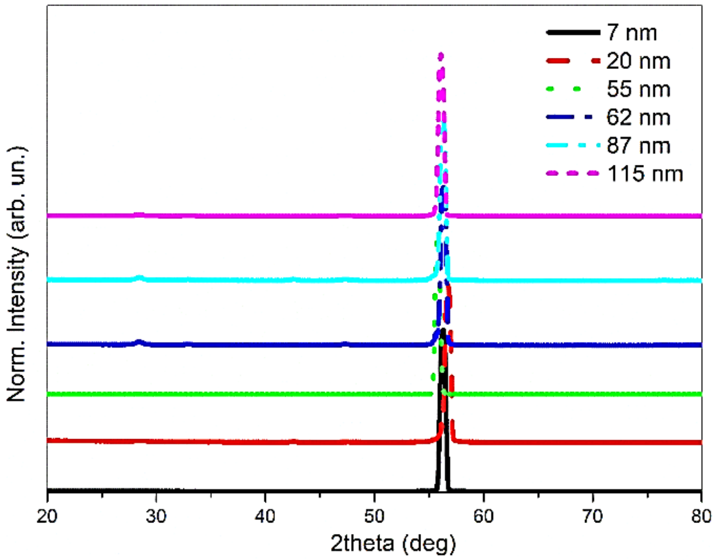

Fig. 1. XRD pattern of the CeO_2 material (colour online)

Table 1. The crystal structure of CeO_2 thin films

Crystal	Thickness	α	β	γ	a	b	c	Geometry	SG
CeO_2	**0.05 M**	**90**	**90**	**90**	**5.014**	**5.014**	**5.014**	**Cubic**	**Fm-3m**
	0.1 M	**90**	**90**	**90**	**5.327**	**5.327**	**5.327**	**Cubic**	**Fm-3m**
	0.2 M	**90**	**90**	**90**	**5.43**	**5.43**	**5.43**	**Cubic**	**Fm-3m**
	0.3 M	**90**	**90**	**90**	**5.425**	**5.425**	**5.425**	**Cubic**	**Fm-3m**
	0.4 M	**90**	**90**	**90**	**5.425**	**5.425**	**5.425**	**Cubic**	**Fm-3m**
	0.5 M	**90**	**90**	**90**	**5.429**	**5.429**	**5.429**	**Cubic**	**Fm-3m**

The observed shifts in the XRD peak positions are primarily attributed to an increase in the lattice parameter, which signifies an expansion of the unit cell dimensions. This lattice expansion can be influenced by several factors, including changes in the chemical composition of the material, which alter the interatomic distances and bonding environment. Additionally, variations in the oxidation states of cerium (Ce^{3+} and Ce^{4+}) within the crystal structure may contribute to these shifts. The coexistence of Ce^{3+} and Ce^{4+} ions, resulting from the redox activity of cerium and its bonding interactions with oxygen, can induce local distortions in the lattice, further affecting the unit cell size and peak positions.

The XRD patterns revealed that the diffraction peaks corresponding to the cubic fluorite phase (space group “Fm-3m”) were less pronounced in thinner films but became more intense and well-defined with increasing film thickness. This trend suggests a thickness-dependent structural evolution, potentially involving a rearrangement or improved crystallinity as the film thickness increases. Thinner films may exhibit a higher degree of disorder or incomplete crystallization due to surface effects and limited atomic mobility during deposition and annealing. In contrast, thicker films benefit from enhanced atomic rearrangement and strain relaxation, leading to a more pronounced cubic phase.

To gain deeper insights into the mechanisms governing the crystal structure and electronic properties of CeO_2 thin films, room-temperature electronic structure calculations were performed using the Density Functional Theory (DFT) code Quantum Espresso (QE). These calculations complement the experimental X-ray absorption spectroscopy (XAS) data and provide a theoretical framework for understanding the electronic behavior of the cubic “Fm-3m” (fluorite-type) CeO_2 material.

The calculated band structure of the cubic CeO_2 material, as shown in Fig. 2, reveals semiconductor properties with an indirect bandgap. The energy bandgap (E_g) was determined to be 1.60 eV, which is consistent with the electronic characteristics of CeO_2 and its potential applications in optoelectronic devices. The density of states (DOS) data, presented in Fig. 3, further elucidates the contributions of cerium 4f, 5d, and oxygen 2p orbitals to the valence and conduction bands. The DOS analysis highlights the hybridization between cerium and oxygen states, which plays a critical role in determining the material's electronic and catalytic properties.

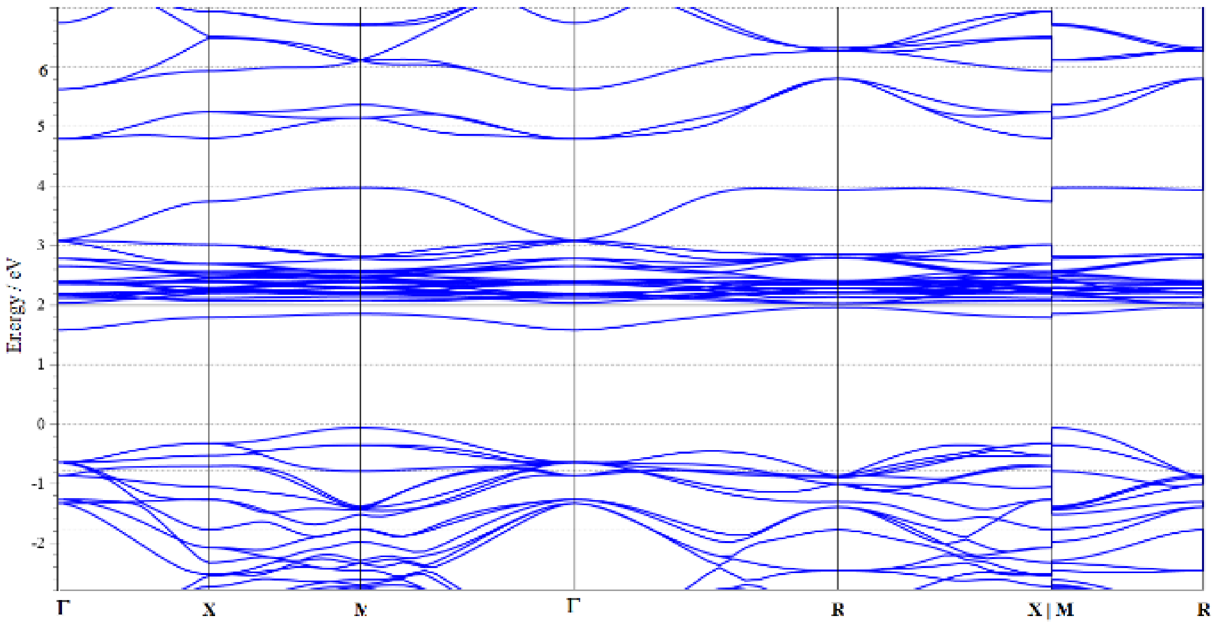

Fig. 2. Band calculation of CeO_2 material (colour online)

Density of states (DOS) analysis reveals a distinct electronic structure in the studied material. The valence band region, located below the Fermi level (E_F), is dominated by oxygen 2p states. Above E_F, in the conduction band, cerium 4f states are prominent. A significant interaction, or hybridization, is observed between these two types of states, with the delocalized Ce 4f orbitals contributing to the oxygen 2p states within the valence band.

The formal electronic configuration of Ce^{4+} is [Xe] $4f^0$ $5d^0$ $6s^0$, indicating the absence of electrons in the 4f, 5d, and 6s orbitals. The presence of these unoccupied orbitals, particularly the 4f orbitals, is crucial in understanding the observed electronic structure. The 4f splitting arises primarily from crystal field effects and electron-electron interactions (specifically, Coulomb and exchange interactions), not directly from the absence of p-electron vacancies. The crystal field, created by the surrounding oxygen ions, breaks the degeneracy of the 4f orbitals. Furthermore, the strong Coulomb repulsion between electrons in the highly localized 4f orbitals leads to further splitting and a high degree of correlation among these electrons. These effects result in the observed localization of the Ce 4f states above E_F.

The 5d orbitals of cerium, while also formally empty in Ce^{4+}, play a vital role in the material's bonding. These 5d orbitals, being less localized than the 4f orbitals, are energetically more favorable for interaction and hybridization with the oxygen 2p orbitals. This interaction leads to the formation of bonding and antibonding molecular orbitals. The statement correctly notes that the d levels are "attracted for bonding with oxygen atoms." This interaction results in a lowering of the 5d band energy, which is reflected in the weak peak structure observed in the lower portion of the conduction band. This feature is attributed to the formation of O 2p-Ce 5d hybridized levels. The observation of this hybridization in X-ray Absorption Spectroscopy (XAS) spectra provides experimental validation of this bonding picture. XAS, being sensitive to the unoccupied electronic states, directly probes the Ce 5d and 4f levels, confirming the presence of the O 2p-Ce 5d hybrid states and the localized nature of the Ce 4f states. The weak intensity of the 5d feature relative to the more prominent 4f signal is consistent with the stronger localization of the 4f orbitals.

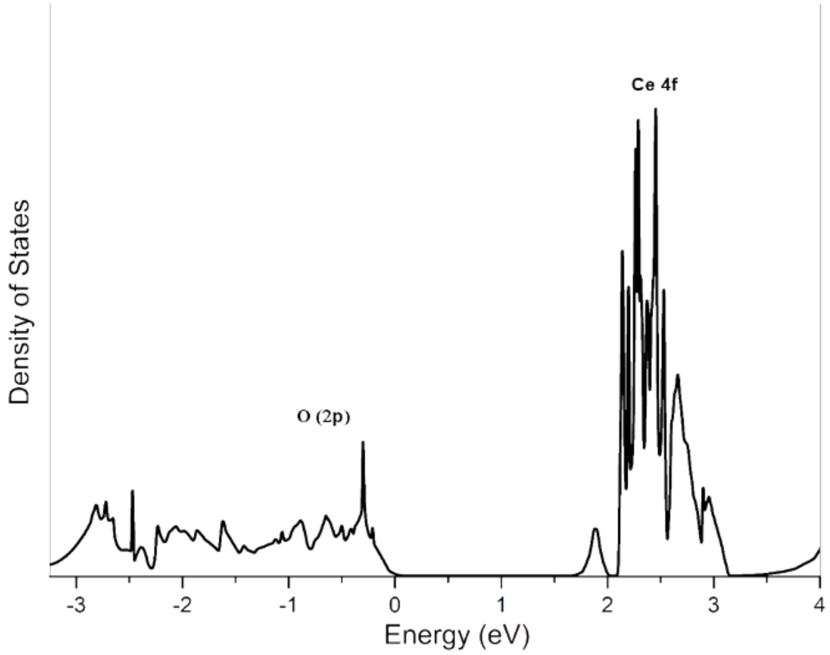

Fig. 3. Density of states (DOS) of CeO_2 material

To elucidate the electronic structure of the CeO_2 material as a function of film thickness, Ce L_3-edge X-ray Absorption Spectroscopy (XAS) data were acquired and are presented in Fig. 4. L_3-edge XAS probes the electronic transitions from the core-level $2p_{3/2}$ electrons to unoccupied states in the conduction band, above the Fermi level (E_F).

The absorption spectra exhibit a weak pre-edge feature "a" at 5715.82 eV. This pre-edge structure is attributed to quadrupole transitions. These transitions involve excitations to hybridized states composed of O 2p and Ce 5d orbitals [15]. The hybridization arises from the interaction between the oxygen 2p orbitals and the cerium 5d orbitals, leading to a mixing of these electronic states. This pre-edge feature provides evidence for the presence of these hybridized states and their contribution to the electronic structure.

The main L_3 absorption edge displays a characteristic doublet peak structure. This doublet structure is a fingerprint of the mixed valence nature of cerium in CeO_2 and is related to the presence of both Ce^{3+} and Ce^{4+}ions. The first peak, labeled (b), is associated with Ce^{3+} ions. The presence of oxygen vacancies in the CeO_2 lattice creates local distortions in the crystal structure and different site symmetries around the cerium ions. These variations in the local environment influence the electronic states of the cerium ions and contribute to the formation of Ce^{3+} species. The second peak, labeled (c), is located at a higher energy than peak (b). This peak is attributed to transitions of the core 2p electrons to the 5d levels in Ce^{4+} ions, where the local environment does not contain oxygen vacancies. The energy separation between peaks (b) and (c) reflects the difference in the electronic structure between Ce^{3+} and Ce^{4+}. The relative intensities of these two peaks are related to the relative concentrations of Ce^{3+} and Ce^{4+} in the material, providing information about the oxidation state and defect concentration in the CeO_2 films. Analyzing the changes in these spectral features with varying film thicknesses allows for a detailed investigation of how the film thickness influences the electronic structure and the relative populations of Ce^{3+} and Ce^{4+} in the CeO_2 material.

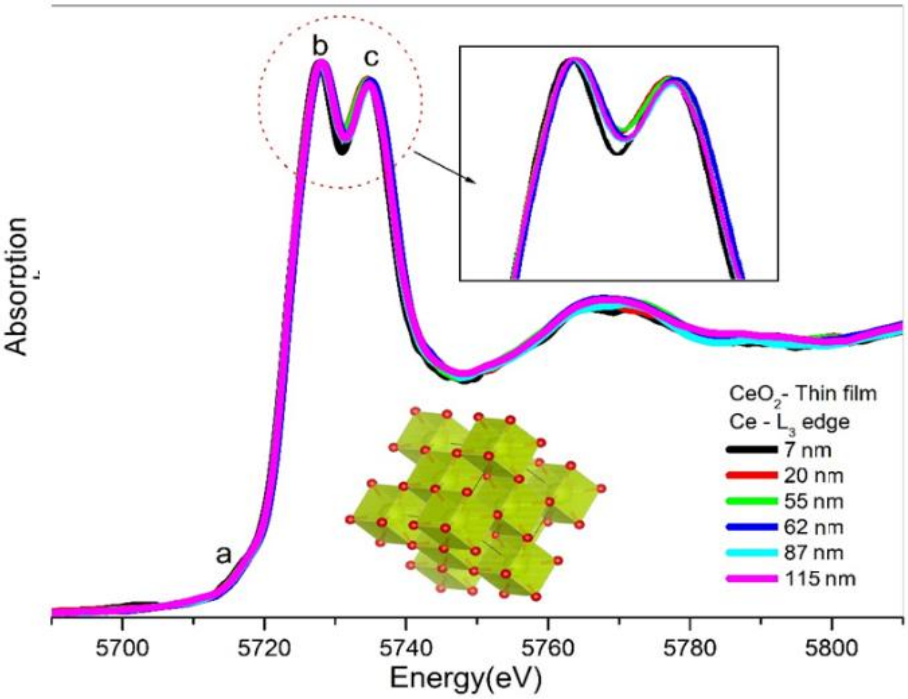

Fig. 4. The Ce L$_3$-edge XANES spectra comparison of the CeO$_2$ thin film series (7 nm, 20 nm, 55 nm, 62 nm, 87 nm, 115 nm) (colour online)

The comparison of spectra in Fig. 4 reveals a high degree of agreement in peak structures, with a noticeable broadening of peak b. This broadening is indicative of an increase in oxygen vacancies as the thickness of the CeO$_2$ films increases. Oxygen vacancies are a common defect in CeO$_2$ due to the material's ability to accommodate non-stoichiometry, particularly in the presence of Ce^{3+} ions, which compensate for the charge imbalance caused by oxygen vacancies. The higher concentration of oxygen vacancies in thicker films leads to a reduction in local site symmetry, as the vacancies disrupt the regular arrangement of oxygen ions in the cubic fluorite structure. This effect is more pronounced in the bulk of the material, where the increased ceria content facilitates the formation of oxygen-deficient regions.

To investigate the local atomic environment and thermal response of CeO$_2$, Extended X-ray Absorption Fine Structure (EXAFS) calculations were performed using the FEFF 8.20 code. EXAFS is a powerful analytical technique that provides detailed insights into the local atomic structure and electronic properties of materials by analyzing the interference patterns generated by the scattering of photoelectrons. When an X-ray photon excites a core electron from the absorbing atom (in this case, cerium), the emitted photoelectron travels through the material and interacts with neighboring atoms. These interactions produce oscillations in the EXAFS signal, which encode information about bond lengths, coordination numbers, and thermal disorder.

The scattering mechanism in EXAFS is governed by Coulombic repulsion between the photoelectrons and the outer-shell electrons of neighboring atoms. As the temperature increases, thermal energy excites electrons from the outer shells, reducing the Coulombic repulsion exerted on the photoelectrons. This reduction in repulsion leads to a decay in the scattering intensity, which can be quantified to assess the temperature-dependent structural and electronic properties of the material.

The most significant finding of this systematic temperature study is the identification of a local structural transition around 400 K. The EXAFS data in both k-space (Fig. 5) and R-space (Fig. 6) show a marked change beyond this temperature, distinct from the gradual changes observed at lower temperatures. This is not a global phase transition, the cubic fluorite structure remains intact, but rather a local rearrangement of the atomic environment around cerium ions. We attribute this transition to the thermal activation of oxygen vacancies, which become mobile and reorganize, leading to the observed distortion in the Ce-O and Ce-Ce coordination shells. This local flexibility is a key materials property, as it governs the kinetics of redox processes and ionic conductivity. The fact that this transition is clearly captured underscores the power of our systematic temperature-dependent EXAFS approach in revealing dynamic processes that are invisible to conventional bulk characterization techniques.

The calculated EXAFS scattering data for CeO$_2$, presented in Fig. 5, compares the material's response at elevated temperatures. The horizontal axis represents the wave vector (k), while the vertical axis represents the scattering intensity. The data reveals two distinct regimes: a collection of similar scattering patterns between 250 K and 400 K, and a significant shift in the data beyond 400 K. This shift and the accompanying asymmetry in the scattering patterns suggest a structural rearrangement induced by oxygen vacancies occurring at temperatures above 400 K. The transition is likely driven by thermal activation, which alters the local atomic environment and electronic interactions within the material.

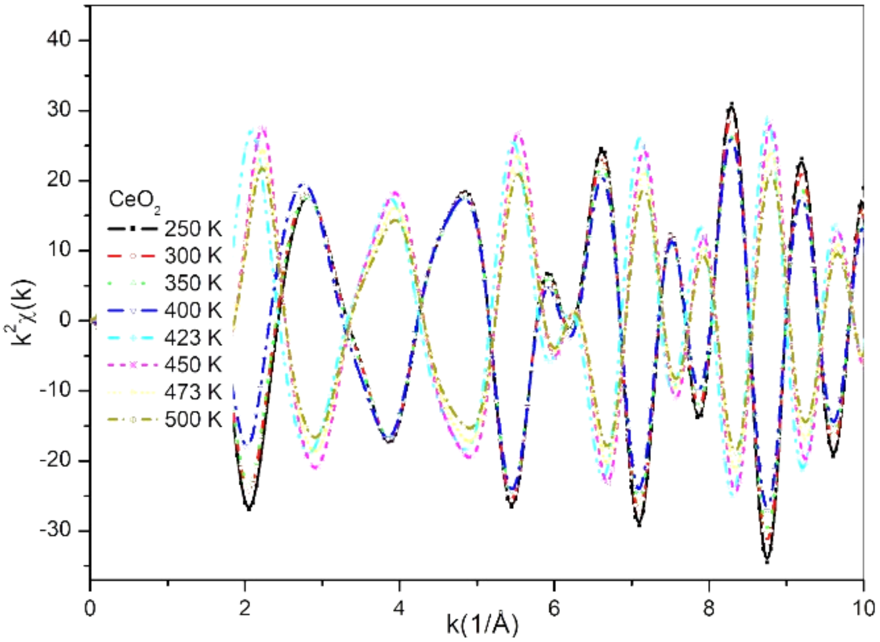

Fig. 5. EXAFS scattering data of Ce L_3-edge XANES spectra comparison at elevated temperatures (colour online)

To gain a more detailed understanding of the atomic-level response to temperature elevation, the real-space representation of the calculated EXAFS data was analyzed using Fourier Transform (FT)-EXAFS, as shown in Fig. 6. FT-EXAFS is a critical analytical tool that converts the oscillatory EXAFS signal from wave vector space (k-space) to real space (R-space). This transformation provides direct insights into the radial distribution of atoms surrounding the absorbing cerium (Ce) atoms, enabling the identification of interatomic distances, coordination numbers, and local structural environments. By analyzing the FT-EXAFS spectra, it is possible to probe subtle changes in the atomic arrangement and bonding dynamics as a function of temperature.

The FT-EXAFS spectrum exhibits a prominent peak corresponding to the first coordination shell of cerium atoms, which consists of eight oxygen (O) atoms at an average distance of 2.343 Å. This peak represents the Ce-O bonds in the cubic fluorite structure of CeO_2. While the positions of the oxygen atoms remain largely consistent, the spectra reveal noticeable disturbances with increasing temperature, particularly above 400 K. These disturbances indicate a reorganization of oxygen atoms around the cerium ions, likely driven by thermal activation and the formation of oxygen vacancies. The dynamic rearrangement of oxygen atoms disrupts the local symmetry and alters the electronic environment of the cerium ions.

The second significant peak in the FT-EXAFS spectrum corresponds to the first cerium coordination shell, consisting of twelve cerium atoms at an average distance of 3.826 Å (Ce-Ce distances). This peak reflects the long-range order and periodic arrangement of cerium ions in the cubic fluorite lattice. Similar to the Ce-O peak, the Ce-Ce peak exhibits subtle shifts above 400 K, further supporting the hypothesis of a temperature-induced structural rearrangement. These shifts are consistent with the changes observed in the k-space EXAFS data (Fig. 5), reinforcing the conclusion that the material undergoes a significant structural transformation at elevated temperatures.

The atomic distances and coordination environments determined from the FT-EXAFS analysis are summarized in Table 2. The data provide quantitative insights into the local structure of CeO_2, including the bond lengths and coordination numbers for both Ce-O and Ce-Ce interactions. The observed changes in these parameters with increasing temperature highlight the material's sensitivity to thermal effects and its propensity for structural reorganization under thermal stress.

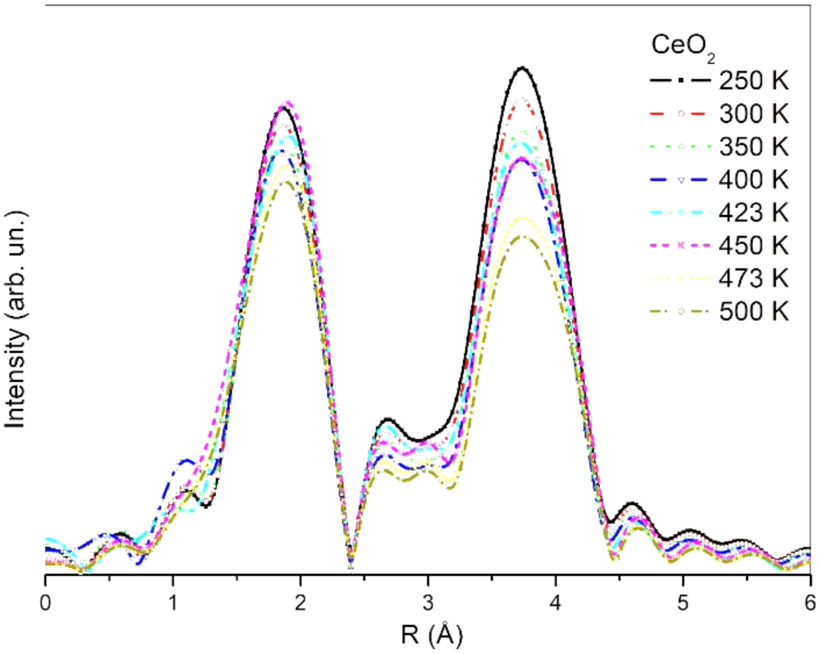

Fig. 6. EXAFS scattering data of Ce L_3-edge XANES spectra comparison at elevated temperatures (colour online)

Table 2. Atomic distances from the source Ce atom in the CeO_2 sample

Sample	Crystal	Source Atom	Atomic Distances	R (Å)	Degeneracy
CeO_2	CeO_2	Ce	Ce-O	2.343	8
			Ce-Ce	3.826	12
			Ce-O	4.487	24
			Ce-O	4.686	8
			Ce-O	4.686	24
			Ce-Ce	5.411	6
			Ce-O	5.897	6

4. Conclusions

In conclusion, this work provides a systematic and multi-faceted investigation into the structural and electronic properties of CeO_2 thin films. By deliberately varying two key parameters, film thickness and temperature, we have uncovered clear and compelling trends. The spin coating method proved to be an effective and economical technique for producing homogeneous CeO_2 films with controlled thicknesses. The thickness-dependent XAS and XRD analyses reveal a progressive increase in oxygen vacancies and lattice relaxation with increasing film thickness. XRD analysis confirmed the cubic fluorite structure of CeO_2, with minor variations in lattice parameters attributed to changes in film thickness and composition. XAS at the Ce L_3-edge revealed the presence of mixed Ce^{3+} and Ce^{4+} oxidation states, with an increase in oxygen vacancies observed in thicker films. Temperature-dependent EXAFS studies identified a local crystal rearrangement transition above 400 K, driven by thermal activation and oxygen vacancy formation, which significantly altered the local atomic environment and electronic interactions. This rearrangement around 400 K demonstrates unexpected local flexibility within a globally stable structure. The local rearrangement is associated with oxygen vacancy formation and partial $Ce^{4+} \rightarrow Ce^{3+}$ reduction, which modifies the hybridization between Ce 4f/5d and O 2p orbitals, which is an important factor governing electronic and catalytic behavior. Besides, such local structural control is the key to tuning redox activity, oxygen vacancy concentration, and thus catalytic, ionic, and electronic functionalities that would greatly enhance the broader impact of the study. This comprehensive approach demonstrates that the electronic structure and defect chemistry of CeO_2 are not static but are dynamically tunable through controlled synthesis and processing conditions, a finding with broad implications for device design.

DFT calculations provided further insights into the electronic structure of CeO_2, confirming an indirect bandgap of 1.60 eV and highlighting the hybridization between Ce 4f/5d and O 2p orbitals. These findings underscore the importance of oxygen vacancies and thermal effects in governing the material's properties. The results demonstrate that CeO_2 thin films exhibit excellent structural stability and tunable electronic properties, making them suitable for a wide range of applications, including catalysis, optoelectronics, and gas sensing. Future work could explore the role of dopants and advanced fabrication techniques to further optimize the performance of CeO_2-based devices.

Ultimately, this study positions CeO_2 not just as a structurally robust material, but as a dynamically tunable one. We have demonstrated that by systematically controlling film thickness and understanding its response to temperature, one can directly engineer its local defect chemistry and electronic structure. The observed thickness-dependent vacancy concentration and the temperature-driven local rearrangement above 400 K are two key levers for controlling its properties. This insight is vital for advancing CeO_2-based technologies. For instance, in catalysis, a higher density of tunable oxygen vacancies enhances activity; in resistive switching devices or gas sensors, the thermal stability of these defects dictates operational longevity and temperature windows. Therefore, this work provides a foundational roadmap for rationally designing CeO_2 thin films with optimized performance for specific advanced technological applications.

References

[1] B.Elidrissi, M. Addou, M. Regragui, C. Monty, A. Bougrine, A. Kachouane, Thin Solid Films **379**(1-2), 23 (2000).

[2] K. Nouneh, R. Hsissou, A. El-Habib, L. El Gana, A. Talbi, M. Beraich, N. Lotfi, M. Addou, Materials Science in Semiconductor Processing **135**, 106049 (2021).

[3] C. Anandan, P. Bera, Applied Surface Science **283**, 297 (2013).

[4] Li Yongheng, S. Weiyu, L. Jian, Z. Zhen, G. Manglai, W. Yuechang, W. Qi, D. Jianlin, Chemical Engineering Journal **330**, 926 (2017).

[5] P. Stefanov, G. Atanasova, D. Stoychev, Ts. Marinova, Surface and Coatings Technology **180**, 446 (2004).

[6] S. Debnath, M. Islam, M. Khan, Bulletin of Materials Science **30**, 315 (2007).

[7] B. Patil, S. Pawar, Journal of Alloys and Compounds **509**(2), 414 (2011).

[8] H.-J. Beie, A. Gnörich, Sensors and Actuators B: Chemical **4**(3-4), 393 (1991).

[9] M. Yamashita, K. Kameyama, S. Yabe, S. Yoshida, Y. Fujishiro, T. Kawai, T. Sato, Journal of Materials Science **37**, 683 (2002).

[10] P. Rajendran, A. Muthuraj, N. E. Rajagounder, Transactions of the Indian Ceramic Society **81**(4), 158 (2022).

[11] S. Zhang, Q. Li, B. Chen, X. Yang., Electrochimica Acta **55**(3), 870 (2010).

[12] Z. Yin, B. Tian, Q. Zhu, C. Duan, Polymers **11**(12), 2033 (2019).

[13] İ. Kanmaz, M. Tomakin, Journal of Sol-Gel Science and Technology **108**(2), 361 (2023).

[14] P. Giannozzi, O. Andreussi, T Brumme, O. Bunau, M. Buongiorno Nardelli, M. Calandra, R. Car, C. Cavazzoni, D. Ceresoli, M. Cococcioni, N. Colonna, I. Carnimeo, A. Dal Corso, S. de Gironcoli, P. Delugas, R. A. DiStasio Jr, A. Ferretti, A. Floris, G. Fratesi, G. Fugallo, R. Gebauer, U. Gerstmann, F. Giustino, T. Gorni, J. Jia, M. Kawamura, H.-Y. Ko, A. Kokalj, E. Küçükbenli, M. Lazzeri, M. Marsili, N. Marzari, F. Mauri, N. L. Nguyen, H.-V. Nguyen, A. Otero-de-la-Roza, L. Paulatto, S. Poncé, D. Rocca, R. Sabatini, B. Santra, M. Schlipf, A. P. Seitsonen, A. Smogunov, I. Timrov, T. Thonhauser, P. Umari, N. Vast, X. Wu, S. Baroni, J. Phys.: Condens. Matter **29**, 465901 (2017).

[15] V. Paidi, D. Brewe, J. Freeland, C. Roberts, J. Van Lierop, Phys. Rev. B **99**, 180403 (2019).

---

[*] Corresponding author: ozkendir@gmail.com